JOURNAL OF GEOPHYSICAL RESEARCH, VOL. 103, NO. D19, PAGES 25,345-25,352, OCTOBER 20, 1998

Stratospheric aerosol surface area and volume inferred from HALOE, CLAES, and ILAS measurements

Mark E. Hervig and Terry Deshler

Department of Atmospheric Science, University of Wyoming, Laramie

Abstract. Relationships are presented for converting remote measurements of stratospheric aerosols to surface area and volume densities. Measurements from the Halogen Occultation Experiment (HALOE), the cryogenic limb array etalon spectrometer (CLAES), and the improved limb atmospheric spectrometer (ILAS) were considered. The relationships were derived using an extensive record of in situ aerosol size distribution measurements made in sulfate aerosols and in polar stratospheric clouds (PSCs). Conversions were derived for sulfate aerosols using the appropriate refractive indices, and for PSCs using the refractive indices for either nitric acid trihydrate or liquid ternary H_2SO_4–H_2O–HNO_3 aerosols. Coincident measurements from HALOE, CLAES, and in situ particle counters are in generally good agreement at middle latitudes, for surface area and volume. Analysis of CLAES measurements under cold polar conditions suggests that these data should be used with caution.

1. Introduction

Physical properties of aerosols such as surface area or volume density can be more desirable than optical properties such as absorption or extinction coefficient. Remote aerosol measurements yield optical properties, and it is therefore useful to quantify the relationships between the optical and physical properties. *Twomey* [1974] concluded that the size distribution moments (surface area and volume) can be reliably inferred from extinctions (absorptions) measured with reasonable uncertainties, and this concept has been validated by numerous investigators [e.g., *Livingston and Russell,* 1989; *Grainger et al.*, 1995]. Here we contribute to these efforts by offering straightforward conversions between aerosol extinction and absorption coefficients and surface area and volume densities. Conversions are presented for stratospheric sulfate aerosols and for polar stratospheric clouds (PSCs) assumed to be composed of either nitric acid trihydrate (NAT) or liquid ternary H_2SO_4–H_2O–HNO_3 aerosols (LTA). The relationships are determined by considering an extensive record of in situ aerosol size distribution measurements from the University of Wyoming balloon-borne optical particle counters (OPCs). The OPCs measure cumulative size distributions, and these data are fit according to lognormal size distributions at height intervals of 0.5 km. Individual instruments can vary, but typically measure radii between 0.01 and 9.5 μm in nine to 13 size intervals (see, for example, *Hofmann and Deshler* [1991]). This work uses profiles measured in stratospheric sulfate aerosols over Laramie, Wyoming (41°N), covering the complete cycle of the Pinatubo volcanic aerosol cloud, and profiles measured in sulfate aerosols and PSCs over McMurdo Station, Antarctica (78°S), during each austral spring from 1989 to 1995 (see, for example, *Deshler et al.* [1993]).

Aerosol measurements from the Halogen Occultation Experiment (HALOE) and the cryogenic limb array etalon spectrometer (CLAES) were considered (both are on the Upper Atmosphere Research Satellite). The HALOE instrument uses satellite solar occultation to measure profiles of solar transmission by the atmosphere's limb, as the Sun rises or sets relative to the spacecraft. Measurements in eight spectral bands between 2.45 and 10 μm are used to retrieve the profiles of seven gas mixing ratios, temperature, and aerosol extinction coefficients at 2.45, 3.40, 3.46, and 5.26 μm wavelengths [*Russell et al.*, 1993; *Hervig et al.*, 1996]. The CLAES instrument measures profiles of thermal emission in nine primary filter regions between 3.5 and 12.9 μm. These measurements are used to retrieve the profiles of 12 gas mixing ratios, temperature, and aerosol absorption coefficients at 5.27, 6.23, 7.96, 10.81, 11.36, 11.86, 12.66, and 12.82 μm wavelengths [*Roche et al.*, 1993; *Massie et al.*, 1996a]. Aerosol surface areas and volumes determined from the CLAES (version 8) and HALOE (version 18) measurements are compared to each other and to the OPC aerosol measurements, as a validation of the measurements and the relationships presented in this work. We have also included conversions for aerosol measurements from the improved limb atmospheric spectrometer (ILAS) instrument on board the Advanced Earth Observing Satellite (ADEOS). ILAS is a solar occultation experiment and retrieves the profiles of six gas mixing ratios, temperature, and aerosol extinction coefficients at 0.78, 7.12, 8.27, 10.60, and 11.76 μm wavelengths [*Mukai et al.*, 1994]. These conversions will facilitate future ILAS studies. ILAS data are not presented or discussed in this work.

There are inherent limitations in satellite limb view observations related to the sample volume dimensions that are often underemphasized in the literature. The sample volume dimensions of a limb viewing instrument are determined by the instantaneous field of view (IFOV) and the geometry of the atmospheric limb path. HALOE and CLAES observations are accurately registered in altitude, and provide vertical resolution of 2 and 2.5 km, respectively. The sample volume length (along the limb) is determined mainly by the vertical resolution, and this dimension is roughly 320 km for HALOE and 360 km for CLAES. The HALOE sample volume width (across the limb) is determined mainly by the angle between the orbit plane and the satellite–Sun vector, and ranges from 6 to 50 km. The CLAES sample volume width (500 km) is a function of the sweep rate and the measurement cycle duration. The large sample volumes are primarily a concern for measurements in

Paper number 98JD01962.
0148-0227/98/98JD-01962$09.00

PSCs, since the horizontal and vertical dimensions of PSCs can often be smaller than the limb view sample volume [e.g., *Deshler et al.*, 1994; *Garcia et al.*, 1995]. For observations of subsample volume scale PSCs, the signals are due to PSC and non–PSC aerosols, and the measured extinctions are therefore less than if the entire volume were filled with PSCs, due to averaging within the sample volume. While this work presents relationships for measurements in PSCs, the reader is advised to use limb–sensor PSC observations with caution.

Aerosol extinction and absorption coefficients can be assumed equal for strongly absorbing particles with radii that are small compared to the wavelength. This is a good assumption for infrared wavelengths and typical aerosol sizes, and many investigators make no distinction between extinction and absorption. In fact, the CLAES absorption coefficients are advertised as extinctions, and have been so labeled by most data users. This work demonstrates that up to 30% differences between extinction and absorption can exist, especially when the aerosols are large, as is the case for the Pinatubo period and for PSCs.

2. Background

The scattering and absorption of radiation by a single spherical particle can be determined from Mie theory as a function of the the particle's size and refractive index, and the wavelength of radiation (λ). For a population of particles, the total extinction (β_E) or absorption (β_A) coefficient is determined by integrating the single–particle cross sections (σ) over the size distribution. The extent to which the relationship between β and the integrated volume (V) is dependent on the size distribution can be visualized by examining the single–particle extinction cross sections, $\sigma_E(\lambda)$, absorption cross sections, $\sigma_A(\lambda)$, and volumes, v. The ratios $\sigma_E(\lambda)/v$ and $\sigma_A(\lambda)/v$ were computed versus radius using the refractive indices for 75 wt.% sulfuric acid solution [*Palmer and Williams*, 1975] at 5.26 and 11.36 μm wavelengths (Figure 1). Fractional aerosol volume distributions representing typical background, volcanic, and PSC conditions are also shown. When the σ–volume relationship is constant over the pertinent range of radius, the relationship between the integrated quantities can be assumed independent of the size distribution. This is a valid assumption for absorption under background and volcanic conditions (Figure 1), as proposed by *Grainger et al.* [1995]. This is clearly not the case for absorption under PSC conditions and for extinction under volcanic and PSC conditions, where the σ–volume ratio shows definite dependence on radius at sizes where the volume contribution can be large. The asymptotic absorption–volume relationship occurs because absorption is proportional to radius cubed when the radius is small compared to the wavelength (i.e., $\varkappa = 2\pi r/\lambda \lesssim 0.25$, the Rayleigh limit). For small values of $\varkappa$, extinction is equal to absorption. The structure at large $\varkappa$ results from resonance in the cross sections with increasing radius, as determined by Mie theory.

In contrast to volume, the relationship between single–particle surface area (s) and σ is not a constant for small $\varkappa$. The ratios $\log_{10}(\sigma_E(\lambda))/\log_{10}(s)$ and $\log_{10}(\sigma_A(\lambda))/\log_{10}(s)$, however, are linear in radius for $\varkappa \lesssim 0.25$ at typical infrared wavelengths. This fact can be used to derive relationships between β and the integrated surface area (S) that are independent of the size distribution for small particles. Although this approach produces good results for measurements in small particles (background aerosols), the errors become large for increasing radii (e.g., volcanic and PSC conditions) and decreasing wavelength, and we pursue the method described below.

3. Moment Conversions

Moment conversions were derived by considering a large body of measured size distributions, giving essentially climatological relationships.

3.1. Sulfate Aerosols

For the case of sulfate aerosols, we have used size distribution profiles measured over Laramie between May 1991 and June 1997 (60 profiles). Extinctions and absorptions were calculated from these size distributions using Mie theory with the refractive indices for sulfate aerosols. The balloon–borne sampling did not include water vapor, and a constant 5 ppmv was assumed to compute the sulfate aerosol composition [*Steele and Hamill*, 1981]. The refractive index versus composition was determined according to *Palmer and Williams* [1975]. The indices were interpolated linearly in H_2SO_4 weight fraction, and adjusted to stratospheric temperatures using the Lorentz–Lorenz (L–L) rule with temperature dependent sulfate solution densities [*Luo et al.*, 1996], as recommended by Palmer and Williams. However, that our treatment of this problem is quite common in the literature does not necessarily justify it. L–L theory applies to indices in the absence of strong absorption features, since these features can shift with temperature and invalidate the simple density (temperature) dependence prescribed by L–L. The validity of the L–L temperature adjustments can only be assessed when measurements of the cold temperature indices become available, and the impact of this effect on our results, therefore, cannot be rigorously determined at this time. However, in wavelength regions with strong absorption features (e.g., 3.5 μm and 10 μm) and in regions with low absorption (e.g., 5 μm), the values of S and V

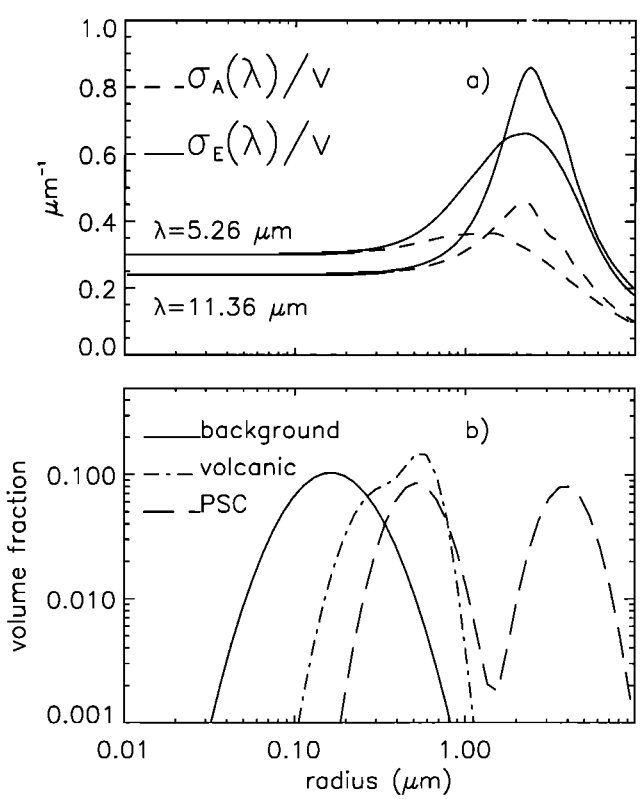

Figure 1. (a) The ratios of extinction to volume ($\sigma_E(\lambda)/v$) and absorption to volume ($\sigma_A(\lambda)/v$) as a function of radius for 75 wt.% sulfuric acid aerosols at 5.26 and 11.36 μm wavelengths. (b) Fractional aerosol volume distributions representing background, volcanic (Pinatubo), and PSC conditions.

inferred below change by less than 5% if the L–L adjustments are not performed. For regions with low absorption these changes are well characterized, and the errors due to L–L should be smaller than the total effect (i.e., less than 5%). No such statement can be made for regions with strong absorption, and our results should be used with this fact in mind.

Contributions from the absorption/extinction peak near 2 μm radius (Figure 1) are greater for some size distributions than for others. Since we have considered many actual size distributions, the resulting relationships can be considered climatological averages. For typical sulfate aerosol sizes, the radius integrals of β and V occur in the size regime where $\sigma(\lambda)/v$ is equal to or greater than the asymptotic value (see Figure 1). As a result, a theoretical (lower) limit of $\beta(\lambda)/V$ can be established by computing $\sigma(\lambda)/v$ versus composition (C) at small radii (i.e., the asymptotic value of $\sigma(\lambda)/v$ in Figure 1). For typical size distributions, ratios of the integrated values ($\beta_E(\lambda)/V$ and $\beta_A(\lambda)/V$) will be equal to or greater than this limit. However, at some wavelengths, for the occasional size distribution containing particles with radii greater than about 2 μm, $\beta_A(\lambda)/V$ can be less than this limit since $\sigma(\lambda)/v$ can be less than the asymptotic value at these sizes (e.g., Figure 1). For illustration, $\beta_E(5.26)/V$ and $\beta_A(5.26)/V$ were computed from the Laramie OPC size distributions, and the results are shown versus composition in Figure 2. The ratios computed from the in situ data were fit in composition to determine conversions to volume (see Figure 2 caption). While the two relationships, $V = f(C, \beta_E)$ and $V = f(C, \beta_A)$, match closely there is notably more scatter for extinction than for absorption, and thus the conversion to volume is more uncertain for extinction than for absorption. These relationships were tested by comparing volumes computed from measured size distributions to volumes predicted from calculated extinctions and absorptions using the relationships in Figure 2, for the Laramie size distributions. The results show that the volume can be predicted to within ±8% using this method for either extinction or absorption, for λ greater than about 3 μm. Figures 1 and 2 illustrate the basic problem and associated uncertainties of relating β and the distribution moments, and also demonstrate some of the differences between extinction and absorption that are often overlooked in the literature.

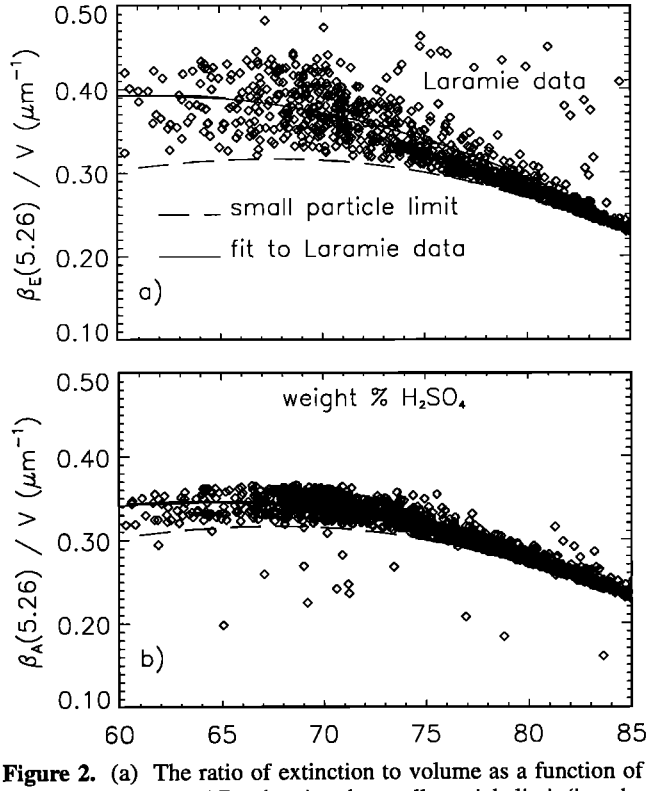

Figure 2. (a) The ratio of extinction to volume as a function of aerosol composition (C), showing the small-particle limit (i.e., the asymptotic value of $\sigma_E(\lambda)/v$ in Figure 1), the values computed from the Laramie size distribution data, and a fit to these data: $V = \beta_E(5.26) \times 1000 \times (23.06 - 0.619C + 0.00447\ C^2)$, for V in $\mu m^3\ cm^{-3}$, β_E in km^{-1}, and C in weight %. (b) As in Figure 2a except the ratio is absorption to volume and the data were fit according to $V = \beta_A(5.26) \times 1000 \times (23.95 - 0.622C + 0.00460\ C^2)$.

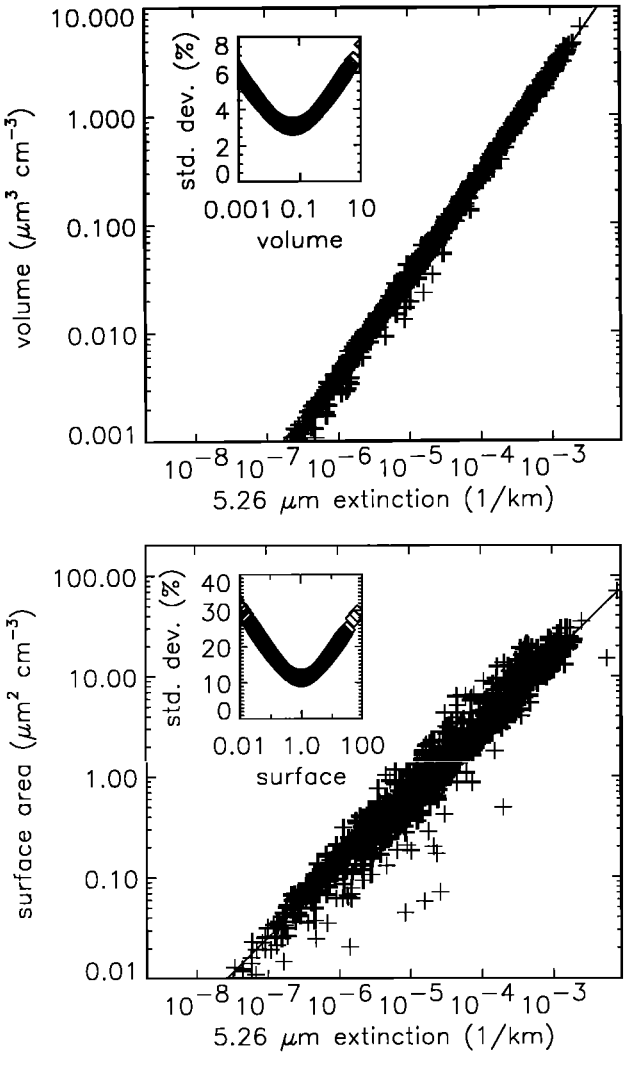

Figure 3. Calculated aerosol volume (or surface area) as a function of calculated 5.26 μm extinction using the Laramie size distributions. A fit to the data points is shown (solid line), and the inset shows the standard deviation of the fit in volume (or surface area).

In a different method, the β versus moments computed from the Laramie size distributions were fit according to

$$M = A\ \beta(\lambda)^B \qquad (1)$$

where M is either S or V, $\beta(\lambda)$ is either the extinction or absorption coefficient, and A and B are constants. For illustration, the relationship between volume and 5.26 μm extinction is shown in Figure 3. The compactness of this relationship (typical for extinction and absorption at wavelengths greater than about 3 μm) is due to the proportionality between absorption and volume, so that variations in both are strongly coupled. Surface area and absorption (or

extinction) are not so strongly coupled and the scatter in similar relationships is therefore greater than for volume (Figure 3). The β–moment relationships for sulfate aerosols were determined according to (1) using the Laramie OPC data, and the constants are reported in Table 1. *Massie et al.* [1996b] have used the method of *Grainger et al.* [1995] to derive conversions for determining surface area and volume from CLAES measurements in sulfate aerosols. The surface areas and volumes derived from CLAES using (1) are within ±10% of the values calculated according to *Massie et al.* [1996b]. *Hervig et al.* [1998] report size distributions retrieved from HALOE multiwavelength measurements of sulfate aerosols, which can be used to calculate S and V. The surface areas and volumes calculated from the HALOE size distributions match the values determined from HALOE using (1) for sulfate aerosols, to within ±20% for pressures greater than 20 mbar, for most latitudes, seasons, and years.

Randomly removing data points from a fit to (1) (e.g., Figure 3) has little or no effect on the slope (the exponent, B); however, this can change the standard deviation of the fit. Since the slope is well determined, uncertainty in the conversions can be assigned to the multiplier (A). The propagation of errors therefore determines that the uncertainty in measured extinction (or absorption), $\delta\beta(\lambda)/\beta(\lambda)$, results in fractional moment uncertainties given by

$$\frac{\delta M}{M} = B\,\frac{\delta\beta(\lambda)}{\beta(\lambda)} + \frac{\delta A}{A} \qquad (2)$$

where $\delta A/A$ is the standard deviation given in the tables.

3.2. PSCs

The size distributions and refractive indices of PSC particles are different than for sulfate aerosols, and thus the β–moment conversions will change for measurements in PSCs. The β–moment relationships in PSCs were investigated using a 7-year record (1989 to 1995) of aerosol size distribution profiles measured in sulfate aerosols and PSCs during the austral spring over McMurdo Station (52 profiles). Calculations with these profiles were made using either the refractive indices for crystalline NAT or those for LTA. The balloon–borne sampling did not include water or nitric acid vapors, and constant mixing ratios were assumed (2 ppmv H_2O and 5 ppbv HNO_3) to determine the equilibrium temperature of NAT (T_{NAT}) [*Hanson and Mauersberger*, 1988] and the equilibrium composition of LTA [*Carslaw et al.*, 1995]. The calculations assuming NAT used all aerosol observations where the temperature was below T_{NAT}, with the NAT refractive indices reported by *Toon et al.* [1994] (wavelengths from about 2 to 20 μm) . As of this writing, the measured indices for LTA covering a complete range of compositions were not available. The indices were determined from existing indices for binary H_2O–H_2SO_4 and H_2O–HNO_3 solutions using the Lorentz–Lorenz mixing rule. This method has been described by *Luo et al.* [1996] for wavelengths from 0.2 to 2 μm, and by *Hervig et al.* [1997] for wavelengths from 5 to 20 μm. The relationships for LTA were determined from data where the calculated equilibrium nitric acid content of the droplets was greater than 10 wt.% (typically temperatures less than about 194 K), using the appropriate calculated indices. The relationships for NAT and LTA have the same form as (1), and the constants are listed in Tables 2 and 3.

4. Results Using HALOE and CLAES

Coincident HALOE, CLAES, and OPC measurements were used to test the surface areas and volumes determined from the CLAES and HALOE measurements.

4.1. Middle Latitude Comparisons

A comparison of HALOE aerosol extinctions with extinctions calculated from the Laramie OPC data showed typical biases of about 25% (HALOE>OPC) and random differences of about 30% [*Hervig et al.*, 1996]. In this work, surface areas, volumes, and effective radii ($3V/S$) determined from the HALOE measurements with (1) were compared to the Laramie OPCs for 17 coincidences found using maximum allowable separations of 48 hours, 2° latitude, and 25° longitude. Comparison statistics for results using the HALOE 3.46 μm channel are shown in Figure 4, and results for the 5.26 and 3.40

Table 1. Constants for Equation (1) for Sulfate Aerosols

	Volume			Surface Area		
Measurement*	A	B	Standard Deviation	A	B	Standard Deviation
β_E(0.78) I	63.65	0.7853	12 to 36%	177.9	0.5835	15 to 47%
β_E(2.45) H	208.7	0.6957	14 to 40%	394.5	0.5096	18 to 53%
β_E(3.46) H	1252.2	0.9752	3 to 10%	1735.2	0.7309	11 to 34%
β_E(5.26) H	1508.3	0.9325	3 to 9%	2002.2	0.6991	11 to 34%
β_A(5.27) C	1847.1	0.9458	2 to 7%	2409.8	0.7122	9 to 31%
β_A(6.23) C	2543.4	0.9562	1 to 5%	3048.7	0.7196	10 to 31%
β_E(7.12) I	2504.3	0.9668	1 to 4%	2992.4	0.7269	10 to 31%
β_A(7.96) C	1591.6	1.018	3 to 11%	2197.3	0.7685	9 to 29%
β_E(8.27) I	1092.5	1.004	2 to 7%	1635.8	0.7568	9 to 30%
β_E(10.61) I	4300.4	1.000	3 to 11%	4337.8	0.7490	11 to 35%
β_A(10.81) C	4273.6	1.012	1 to 5%	4452.2	0.7602	10 to 32%
β_A(11.36) C	2072.6	0.9389	2 to 8%	2602.6	0.7062	10 to 31%
β_E(11.76) I	2494.3	0.9121	5 to 17%	2871.4	0.6825	12 to 37%
β_A(11.86) C	2830.2	0.9125	3 to 12%	3268.1	0.6858	10 to 33%
β_A(12.66) C	3131.3	0.9028	4 to 13%	3542.6	0.6789	10 to 32%
β_A(12.82) C	3220.9	0.9052	4 to 12%	3621.0	0.6807	10 to 32%

Constants are based on units of km^{-1} for extinction and absorption, $\mu m^3\ cm^{-3}$ for volume, and $\mu m^2\ cm^{-3}$ for surface area. The low and high range of the standard deviation of each fit are given (e.g., inset of Figure 3). The constants were determined using 1172 distributions. The constants for the HALOE 3.46 μm channel can be used for the 3.40 μm measurements.

*H denotes HALOE, C denotes CLAES, and I denotes ILAS.

Table 2. Constants for Equation (1) for NAT PSCs

	Volume			Surface Area		
Measurement*	*A*	*B*	Standard Deviation	*A*	*B*	Standard Deviation
β_E(2.45) H	169.1	0.6878	19 to 74%	140.2	0.4249	25 to 96%
β_E(3.46) H	1004.8	0.9458	7 to 25%	597.4	0.6261	18 to 63%
β_E(5.26) H	1487.9	0.9840	4 to 16%	815.6	0.6575	17 to 58%
β_A(5.27) C	2225.2	1.008	6 to 22%	1297.5	0.6965	13 to 47%
β_A(6.23) C	2864.3	1.001	4 to 15%	1376.8	0.6787	15 to 53%
β_E(7.12) I	1897.1	0.9819	4 to 15%	881.2	0.6480	18 to 62%
β_A(7.96) C	2206.8	0.9976	5 to 19%	1142.7	0.6752	15 to 55%
β_E(8.27) I	1446.1	0.9519	8 to 30%	649.0	0.6119	20 to 71%
β_E(10.60) I	1873.5	0.8783	14 to 52%	599.2	0.5391	24 to 91%
β_A(10.81) C	6191.6	0.9737	4 to 15%	1829.5	0.6263	18 to 67%
β_A(11.36) C	5779.3	0.9821	3 to 12%	1825.8	0.6460	18 to 64%
β_E(11.76) I	2837.7	0.9441	7 to 29%	967.9	0.6034	21 to 77%
β_A(11.86) C	5073.1	0.9927	2 to 8%	1777.6	0.6591	17 to 60%
β_A(12.66) C	5173.1	0.9913	2 to 8%	1783.7	0.6572	17 to 61%
β_A(12.82) C	5130.5	0.9939	2 to 7%	1803.8	0.6607	17 to 60%

Units and standard deviations are as described in Table 1. The constants were determined using 1010 distributions and there are no constants for the shortest ILAS wavelength. The constants for the HALOE 3.46 μm channel can be used for the 3.40 μm measurements.

*H denotes HALOE, C denotes CLAES, and I denotes ILAS.

μm channels are similar. HALOE–OPC comparisons for the 2.45 μm channel show mean differences of ±20% in surface area and volume at pressures greater than 40 mbar, with increasing systematic differences (HALOE>OPC) at lower pressures. These differences are consistent with the HALOE–OPC extinction comparisons reported by *Hervig et al.* [1996] and the HALOE–OPC surface area and volume comparisons reported by *Hervig et al.* [1998].

A validation of the CLAES aerosol measurements by *Massie et al.* [1996a] compares the measured absorption coefficients to extinctions calculated from the Laramie OPC data. These results show the best CLAES–OPC agreement for the 10.81 and 11.36 μm wavelengths, with large systematic differences (CLAES>OPC) for the other channels. In this work, surface areas, volumes, and effective radii determined from CLAES were compared to the OPCs for six coincidences over Laramie during 1992–1993. These comparisons were consistent with *Massie et al.* [1996a], showing the best CLAES–OPC agreement for the 11.36 and 10.81 μm channels. Statistics for comparisons using the CLAES 11.36 μm channel are shown in Figure 5. Both the surface area and volume comparisons have mean differences less than ±30% for pressures greater than ~30 mbar, and random differences of about 30% over the comparison vertical extent.

Surface areas and volumes determined from CLAES and HALOE were compared for 50 coincidences near 43° N during January 1993. Statistics are shown in Figure 6 for comparisons of surface area determined from the HALOE 3.46 and 5.26 μm channels and the CLAES 10.81 and 11.36 μm channels. The two HALOE channels agree to within 5% for pressures greater than 20 mbar, and the two CLAES channels are typically within 20% of HALOE. Surface areas determined from the other CLAES channels (not shown) are

Table 3. Constants for Equation (1) for LTA PSCs

	Volume			Surface Area		
Measurement*	*A*	*B*	Standard Deviation	*A*	*B*	Standard Deviation
β_E(0.78) I	144.3	0.8280	26 to 105%	229.7	0.5998	21 to 85%
β_E(5.26) H	1888.5	0.9571	10 to 37%	851.9	0.6284	30 to 114%
β_A(5.27) C	3830.0	1.006	6 to 22%	1739.6	0.6890	24 to 90%
β_A(6.23) C	3084.1	0.9993	6 to 24%	1489.3	0.6835	24 to 88%
β_E(7.12) I	2025.6	0.9814	7 to 28%	988.8	0.6567	28 to 100%
β_A(7.96) C	2624.4	1.015	8 to 33%	1462.7	0.7056	22 to 82%
β_E(8.27) I	1701.3	0.9839	10 to 38%	909.9	0.6625	27 to 104%
β_E(10.60) I	2357.4	0.9503	12 to 46%	914.8	0.6155	32 to 118%
β_A(10.81) C	4407.3	0.9961	4 to 16%	1719.8	0.6702	26 to 98%
β_A(11.36) C	4251.5	0.9949	9 to 34%	1654.3	0.6678	27 to 104%
β_E(11.76) I	2274.9	0.9298	15 to 57%	842.9	0.5957	34 to 124%
β_A(11.86) C	5075.1	0.9861	6 to 24%	1777.4	0.6568	28 to 104%
β_A(12.66) C	6346.4	0.9698	12 to 44%	1978.9	0.6416	30 to 110%
β_A(12.82) C	6524.7	0.9665	13 to 50%	2010.6	0.6392	30 to 111%

Units and standard deviations are as described in Table 1. The constants were determined using 398 distributions and there are no constants for the shortest HALOE wavelengths.

*H denotes HALOE, C denotes CLAES, and I denotes ILAS.

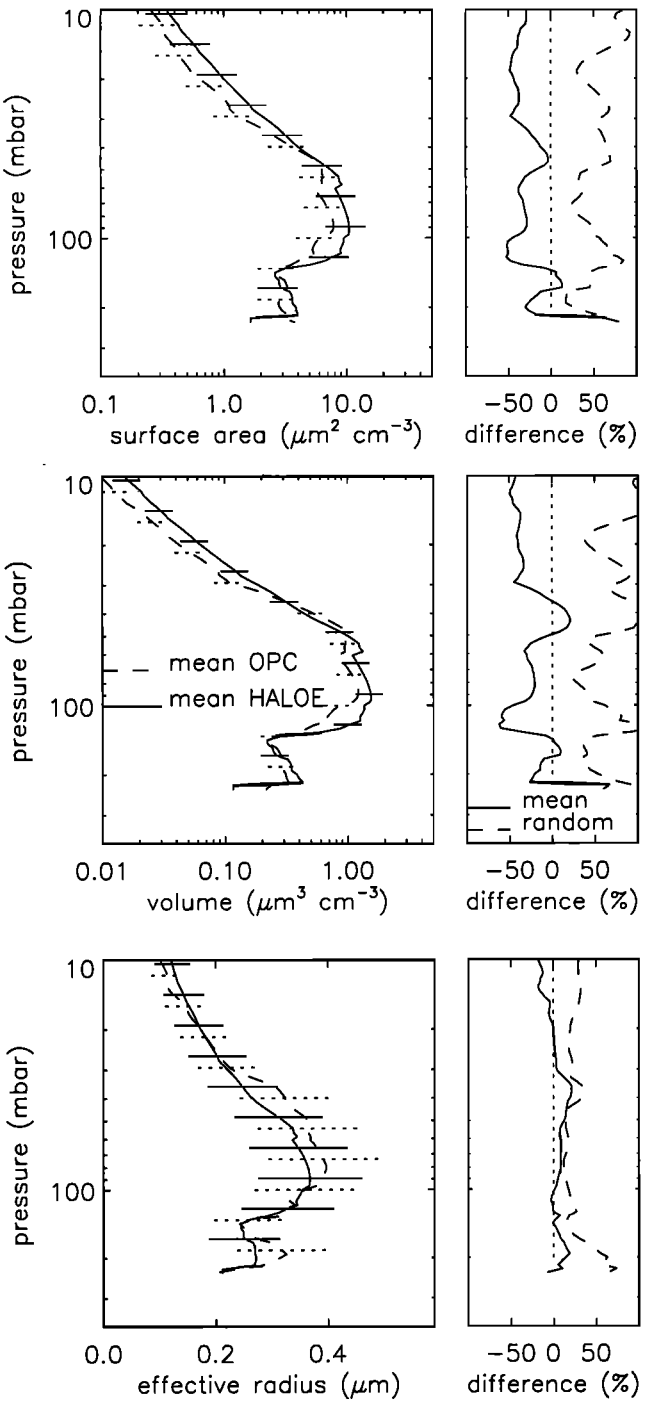

Figure 4. Aerosol surface area, volume, and effective radius determined from the HALOE 3.46 μm channel using (1) for sulfate aerosols, compared to OPC measurements over Laramie. Statistics for the 17 coincident HALOE and OPC profiles are shown as mean profiles, mean differences, and random differences (standard deviation of the difference). The average HALOE–OPC separations were 20.1 hours, 0.7° latitude, and 7.1° longitude.

systematically greater than HALOE by over 30%. The volume comparisons are similar to the surface area comparisons.

4.2. Antarctic Comparisons

HALOE and CLAES do not sample concurrently under PSC conditions. There were five CLAES–OPC coincidences over McMurdo Station (78°S) during the austral spring of 1992 (average separations of 7 hours and 113 km) and no HALOE–OPC coincidences over McMurdo to date. The McMurdo comparisons serve to test the CLAES measurements under cold polar conditions. Additionally, it is necessary to assume a particle type to infer the surface and volume under PSC conditions, and these assumptions can be tested for measurements where the PSC type is known. Using the OPC data with coordinated lidar measurements over McMurdo, *Adriani et al.* [1995] have identified PSCs as either solid (depolarizing) or liquid (nondepolarizing) and have inferred the

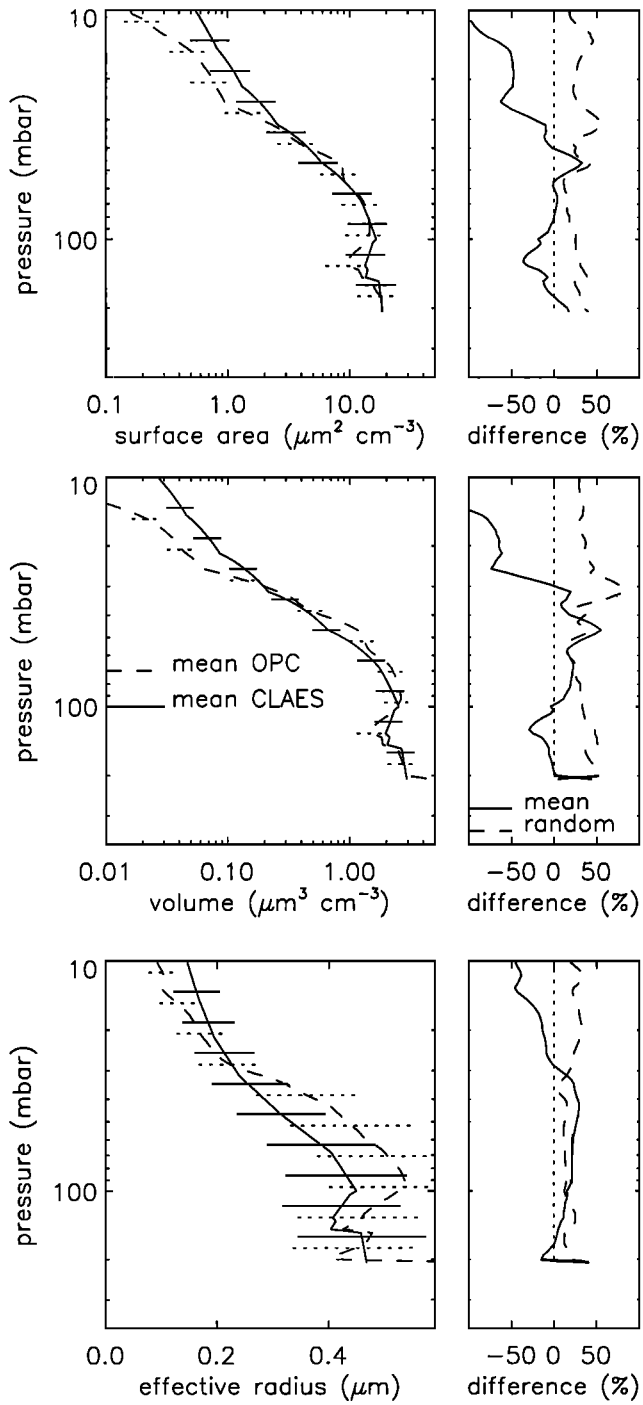

Figure 5. Aerosol surface area, volume, and effective radius determined from the CLAES 11.36 μm channel using (1) for sulfate aerosols, compared to OPC measurements over Laramie. Statistics for the six coincident CLAES and OPC profiles are shown as mean profiles, mean differences, and random differences (standard deviation of the difference). The average CLAES–OPC separations were 14 hours, 0.7° latitude and 6.8° longitude.

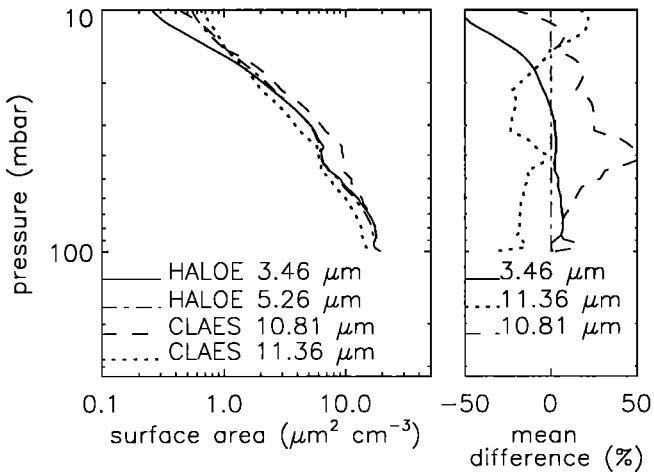

Figure 6. Comparison of aerosol surface areas determined from the HALOE 3.46 and 5.26 μm channels with surface areas determined from the CLAES 10.81 and 11.36 μm channels, for 50 coincidences between 35°N and 45°N during January 1993. The average HALOE–CLAES separations were 6.7 hours, 0.9° latitude, and 10.1° longitude. The statistics are shown as (left) mean profiles, and mean (right) differences from the surface area determined from the HALOE 5.26 μm channel.

composition through estimations of the refractive index. Volumes inferred from the CLAES 11.86 μm channel for the sulfate, NAT, and LTA assumptions are compared to coincident OPC measurements on August 31, 1992, in Figure 7. The NAT equilibrium temperatures are also shown in Figure 7. The CLAES volumes computed assuming NAT and LTA are nearly identical, and are less than the CLAES volumes computed assuming sulfate. The OPC temperatures are near or below T_{NAT} for pressures greater than ~50 mbar, and an analysis of the coincident OPC and lidar measurements on this day suggested that these layers were composed of NAT [*Adriani et al.*, 1995]. While the CLAES–OPC comparison does not suggest a particle type, given the respective uncertainties, the overall agreement is good, regardless of the composition assumption (the surface area comparisons are similar).

At 11.86 μm, the volumes inferred for assuming PSCs are smaller than the volumes inferred for assuming sulfate aerosols. While this may seem curious, it should be noted that this result is consistent with the refractive indices and with optical theory, and that for other wavelengths this result can be reversed. We do not imply that the sulfate volumes which correlate to observed PSC absorptions are real. Rather, it should be noted that for a given aerosol absorption (or extinction), the volume (or surface area) of aerosol which correlates to that absorption will vary according to the aerosol type.

Figure 8 shows the CLAES–OPC comparison for August 29, 1992 (as in Figure 7). This comparison shows large systematic differences in volume (CLAES>OPC) and in temperature (CLAES<balloon) over the comparison vertical extent. The CLAES temperatures are from 3 to 8 K colder than the in situ data, in contrast to Figure 7 where the differences alternate (±3 K). The results in Figure 8 are more typical of the five CLAES–OPC coincidences than the results shown in Figure 7. Statistically, the CLAES volumes (and surface areas) are greater than the OPCs by 30% to 90% at pressures from 100 to 20 mbar, respectively, for all channels except the 11.86 and 7.96 μm channels. The 11.86 and 7.96 μm channels are within ±10% of the OPCs for pressures greater than 70 mbar, with large systematic differences (CLAES > OPC) at lower pressures.

Comparing the CLAES and in situ temperature profiles over McMurdo reveals that the CLAES temperatures are typically colder at pressures from 100 to 20 mbar. Since CLAES measures thermal emission, the measurement retrievals rely on accurate temperature information. The sensitivity of blackbody radiance to temperature increases at low temperatures and for increasing optical thickness, as determined by the Planck function. Test calculations show that a 5 K cold bias can produce up to 40% overestimation of the absorption coefficient (depending on the optical thickness, wavelength, and temperature). The CLAES–OPC bias, however, is 90% in some instances, and other effects should be explored. As previously discussed, the horizontal and vertical dimensions of PSCs can often be smaller than the CLAES sample volume dimensions (2.5 km vertical×360 km along limb ×500 km across limb), and it is possible that the CLAES measurements were from an average of PSC and non–PSC aerosols, both within the same sample volume. However, this effect would result in an overall decrease in the measured PSC absorption coefficients, and it is therefore an unlikely explanation since the CLAES measurements were greater than the OPCs. The episodic nature of PSCs places high demands on the selection of coincident measurements, and it is possible that the CLAES–OPC coincidences are comparing PSC with non–PSC observations, even though the time and space separations were small.

5. Conclusions

Using an extensive record of in situ size distribution measurements in sulfate aerosols and PSCs, relationships were determined for converting extinction or absorption coefficients to surface area and volume densities. One advantage of these relationships is that results can be easily obtained by investigators using the HALOE, CLAES, or ILAS data sets. Validations at middle latitudes suggest that all four HALOE channels can be used to reliably infer the surface area and volume at pressures greater than 20 mbar. Middle latitude comparisons using CLAES suggest that the 11.36 and 10.81 μm channels can be used to reliably infer the surface area and volume at pressures greater than 30 mbar. The surface areas and volumes inferred from the other CLAES channels show large systematic differences (CLAES larger) when compared to the OPCs and to HALOE. CLAES–OPC comparisons under PSC conditions

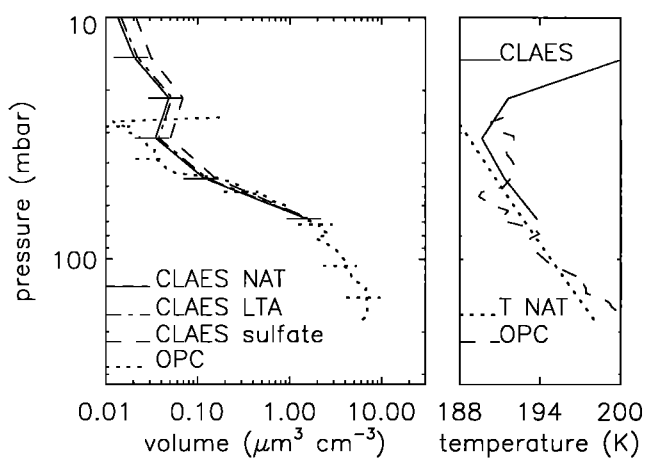

Figure 7. OPC measurements over McMurdo Station (77.8°S, 166.7°E) and coincident CLAES measurements (77.9°S, 177.2°E), on August 31, 1992. The measurements were separated by 7.9 hours and 129.6 km great circle distance. (left) Volumes determined from the CLAES 11.86 μm aerosol measurements using (1) and assuming NAT, LTA, and sulfate, compared to the OPC measurements. Error bars are shown for the CLAES NAT profile and the OPC profile. (right) The CLAES and balloon temperatures and T_{NAT} computed from the balloon profile assuming constant 2 ppmv H_2O and 5 ppbv HNO_3.

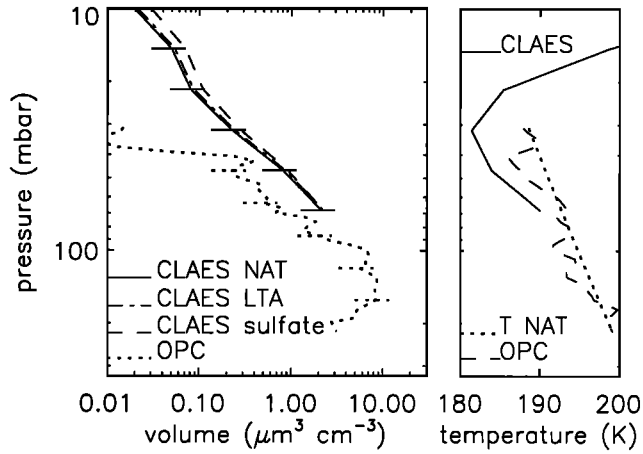

Figure 8. As in Figure 7 except for measurements on August 29, 1992. The CLAES measurements were at 77.4°S, 162.4°E, and the CLAES–OPC separations were 6.4 hours and 112.4 km great circle distance.

show the best agreement for the CLAES 11.86 and 7.96 μm channels; however, good agreement is only obtained for pressures typically between 70 and 100 mbar, and all the CLAES channels exhibit large systematic differences (CLAES>OPC) at lower pressures. The McMurdo results are inconsistent with the middle latitude comparisons, and this effect is the topic of ongoing investigations.

Acknowledgments. This work was supported through funding from the NASA Langley Research Center, the UARS Guest Investigator Program, and the National Science Foundation.

References

Adriani, A., T. Deshler, G. Di Donfrancesco, and G. P. Gobbi, Polar stratospheric clouds and volcanic aerosol during spring 1992 over McMurdo Station, Antarctica: Lidar and particle counter comparisons, *J. Geophys. Res., 100*, 25,877–25,897, 1995.

Carslaw, K. S., B. P. Luo, and T. Peter, An analytic expression for the composition of aqueous HNO_3–H_2SO_4 stratospheric aerosols including gas phase removal of HNO_3, *Geophys. Res. Lett., 22*, 1877–1880, 1995.

Deshler, T., B. J. Johnson, and W. R. Rozier, Balloonborne measurements of Pinatubo aerosol during 1991 and 1992 at 41°N: Vertical profiles, size distributions, and volatility, *Geophys. Res. Lett., 20*, 1435–1438, 1993.

Deshler, T., B. J. Johnson, and W. R. Rozier, Changes in the character of polar stratospheric clouds over Antarctica in 1992 due to the Pinatubo volcanic aerosol, *Geophys. Res. Lett.*, 21, 273–276, 1994.

Garcia, O., K. Pagan, P. Foschi, S. Gaines, and R. S. Hipskind, Detection of polar stratospheric clouds over Antarctica using AVHRR images obtained at Palmer Station during August 1992, *Polar Record, 31*, 211–226, 1995.

Grainger, R. G., A. Lambert, C. D. Rodgers, F. W. Taylor, and T. Deshler, Stratospheric aerosol effective radius, surface area and volume estimated from infrared measurements, *J. Geophys. Res., 100*, 16,507–16,518, 1995.

Hanson, D., and K. Mauersberger, Laboratory studies of the nitric acid trihydrate: Implications for the south polar stratosphere, *Geophys. Res. Lett., 15*, 855–858, 1988.

Hervig, M. E., J. M. Russell III, L. L. Gordley, J. Daniels, J. H. Park, S. R. Drayson, and T. Deshler, Validation of aerosol measurements made by the Halogen Occultation Experiment, *J. Geophys. Res., 101*, 10,267–10,275, 1996.

Hervig, M. E., T. Deshler, and J. M. Russell III, Aerosol size distributions obtained from HALOE spectral extinction measurements, *J. Geophys. Res., 103*, 1573–1583, 1998.

Hervig, M. E., K. S. Carslaw, T. Peter, T. Deshler, L. L. Gordley, G. Redaelli, U. Biermann, and J. M. Russell III, Polar stratospheric clouds due to vapor enhancement: HALOE observations of the Antarctic vortex in 1993, *J. Geophys. Res., 102*, 28,185–28,193, 1997.

Hofmann, D. J., and T. Deshler, Stratospheric cloud observations during the formation of the Antarctic ozone hole in 1989, *J. Geophys. Res., 96*, 2897–2912, 1991.

Livingston, J. M., and P. B. Russell, Retrieval of size distribution moments from multiwavelength particulate extinction measurements, *J. Geophys. Res., 94*, 8425–8433, 1989.

Luo, B. P., U. K. Krieger, and T. Peter, Densities and refractive indices of H_2SO_4 /HNO_3 /H_2O solutions to stratospheric temperatures, *Geophys. Res. Lett., 23*, 3707–3710, 1996.

Massie, S. T., et al., Validation studies using multiwavelength cryogenic limb array etalon spectrometer (CLAES) observations of stratospheric aerosols, *J. Geophys. Res., 101*, 9757–9773, 1996a.

Massie, S. T., T. Deshler, G. Thomas, J. Mergenthaler, and J. M. Russell III, Evolution of the inferred properties of the Mount Pinatubo aerosol cloud over Laramie, Wyoming, *J. Geophys. Res.*, 23,007–23,019, 1996b.

Mukai, S., I. Sano, Y. Sasano, M. Suzuki, and T. Yokota, Retrieval algorithms for stratospheric aerosols based on ADEOS/ILAS measurements, *IEEE Trans. Geosci. Remote Sens., 32*(5), 1124–1127, 1994.

Palmer, K. F., and D. Williams, Optical constants of sulfuric acid: Application to the clouds of Venus?, *Appl. Opt., 14*, 208–219, 1975.

Roche, A. E., J. B. Kumer, J. L. Mergenthaler, G. A. Ely, W. G. Uplinger, J. F. Potter, T. C. James, and L. W. Sterritt, The cryogenic limb array etalon spectrometer (CLAES) on UARS: Experiment description and performance, *J. Geophys. Res., 98*, 10,763–10,775, 1993.

Russell, J. M., III, L. L. Gordley, J. H. Park, S. R. Drayson, W. D. Hesketh, R. J. Cicerone, A. F. Tuck, J. E. Frederick, J. E. Harries, and P. J. Crutzen, The Halogen Occultation Experiment, *J. Geophys. Res., 98*, 10,777–10,797, 1993.

Steele, H. M., and P. Hamill, Effects of temperature and humidity on the growth and optical properties of sulfuric acid–water droplets in the stratosphere, *J. Aerosol Sci., 12*, 517–528, 1981.

Toon, O. B., M. A. Tolbert, B. G. Koehler, A. M. Middlebrook, and J. Jordan, Infrared optical constants of H_2O ice, amorphous nitric acid solutions, and nitric acid hydrates, *J. Geophys. Res., 99*, 25,631–25,645, 1994.

Twomey, S., Information content in remote sensing, *Appl. Opt., 13*, 942–945, 1974.

T. Deshler and M.E. Hervig (corresponding author), Department of Atmospheric Science, University of Wyoming, P.O. Box 3038, Laramie, WY 82071. (e-mail: hervig@trex.uwyo.edu)

(Received October 24, 1997; revised June 3, 1998;
accepted June 3, 1998.)